Annals of Diagnostic Pathology 41 (2019) 14–23

Contents lists available at ScienceDirect

Annals of Diagnostic Pathology

journal homepage: www.elsevier.com/locate/anndiagpath

Original Contribution

Magnifying glass on spiradenoma and cylindroma histogenesis and tumorigenesis using systematic transcriptome analysis

Achim H. Bell[a], Victor G. Prieto[b], Renata Ferrarotto[d], Ryan P. Goepfert[c], Jeffrey N. Myers[c], Randal Weber[c], Diana Bell[b,c,*]

[a] Department of Research Pathology, MD Anderson Cancer Center, 1515 Holcombe Blvd., Houston, TX 77030, USA
[b] Department of Pathology, MD Anderson Cancer Center, 1515 Holcombe Blvd., Houston, TX 77030, USA
[c] Department of Head and Neck Surgery, MD Anderson Cancer Center, 1515 Holcombe Blvd., Houston, TX 77030, USA
[d] Department of Thoracic Head and Neck Oncology, MD Anderson Cancer Center, 1515 Holcombe Blvd., Houston, TX 77030, USA

ABSTRACT

Spiradenoma and cylindroma are related sweat gland tumors. To delineate their histogenesis, gene profiles, and their potential drivers, we performed a whole-transcriptome sequencing analysis of fourteen samples of spiradenoma/cylindroma in comparison to normal samples.

A total of 12 spiradenomas, 5 cylindromas, 3 hybrid spiradenomas/cylindromas and 2 adnexal carcinomas were included in this study.

1335 characteristic genes and transcripts expressed over all 14 spiradenoma/cylindroma tumors were identified, and two groups of expression profiles were observed.

Highest upregulated top 7 gene signatures characterized benign tumors with developmental and differentiation related genes, and carcinomas with top 7 genes mainly related to signaling, reorganization and metabolism of membranes.

Immunohistochemistry of protein expressions validated 4 upregulated genes (ODAM, HOXB13, MYB and SOX10) considered important and as potential biomarkers for spiradenomas and cylindromas.

We further compared the transcriptome of eccrine adnexal tumors with the transcriptome of adenoid cystic carcinoma (ACC) to identify the overlapping genes that may indicate histogenesis. There were 36 specific genes overlapping between adnexal carcinomas and the epithelial-dominant subtype of ACC, and 27 specific genes overlapping benign adnexal tumors with the myoepithelial-dominant subtype of ACC, At this point there is no known specific biomarker to aid in the diagnosis of eccrine spiradenoma and cylindroma in small samples or biopsies within the context of morphological overlap with ACC.

In conclusion, spiradenomas and cylindromas are characterized by overexpressed developmental genes, where LHX2 and activated WNT signaling possibly drive associated carcinomas.

1. Introduction

Eccrine spiradenoma and cylindroma are closely related tumors [1-3]. They overlap morphologically, and hybrid tumors with spiradenomatous and cylindromatous components are encountered [4-7]. The majority of spiradenoma and cylindroma are solitary neoplasms; however, there may be multiple tumors in the setting of the Brooke-Spiegler syndrome [1,2,8-11].

Malignant transformation in spiradenoma, cylindroma, and cylindroma-spiradenoma hybrids is rare, with about 200 cases documented in the literature [12-16]. The malignant component covers a wide morphological spectrum from frank invasive adenocarcinoma to a more subtle appearance that is similar to that of basal cell adenocarcinoma of the salivary glands [9,16-19]. The malignant neoplasms have been histologically divided into low- and high-grade. The low-grade malignant tumors are diagnostically challenging, with loss of a dual cell population, increased mitotic activity, and limited cytological atypia [9,16]. The differential diagnosis of morphologically low-grade spiradenocarcinoma is wide and relies on the identification and sampling of its benign counterpart [9,16]. Primary cutaneous Adenoid cystic carcinoma (ACC), for instance, shows many overlapping histological features with low-grade spiradenocarcinoma, however, it has a more diffuse infiltrative growth pattern, and prominent perineural invasion [10,16,20]. Cutaneous metastasis from a salivary gland primary tumor is also an important differential consideration [9,10,16].

Irrespective of the terminology, the majority of tumors have indolent biological behavior, with benign morphologic features and slow local growth [7,10,16]. Their rarity r have precluded a standardized treatment approach but the treatment of choice for spiradenocarcinomas is complete surgical removal and follow-up [7,10,16].

In this retrospective study, we performed an in-depth analysis of the transcriptomes of adnexal eccrine tumors, and thus find and classify

* Corresponding author at: Department of Pathology, MD Anderson Cancer Center, 1515 Holcombe Blvd., Houston, TX 77030, USA.
E-mail address: diana.bell@mdanderson.org (D. Bell).

https://doi.org/10.1016/j.anndiagpath.2019.04.015

potential drivers of these tumor types. To our knowledge, this is the first RNAseq analysis of these neoplasms.

2. Material and methods

2.1. Patients

Patients were identified from the pathology archives at The University of Texas MD Anderson Cancer Center (Houston, Texas), with institutional review board approval. Diagnosis was confirmed independently by two experienced, subspecialized dermatopathologist (VGP) and a head and neck pathologist (DB).

2.2. Tissue specimens

Primary adnexal FFPE tumor specimens were available for 22 patients with annotated clinical outcome data. Microdissected adnexal structures from 7 non-matching normal FFPE skin tissues samples (from breast revisions) were analyzed in parallel.

2.3. RNA-Seq sample preparation and sequencing

For RNA-Seq, total RNA from FFPE tissue sections of 14 adnexal tumor (7 spiradenomas, 2 cylindromas, 3 hybrid spiradenomas/cylindromas, and 2 adnexal carcinomas) and 7 normal skin specimens was extracted using the High Pure FFPET RNA Isolation Kit (Roche Sequencing Solutions, Pleasanton, CA, USA), according to the manufacturer's instructions. Total RNA quality and quantity were verified spectrophotometrically (NanoDrop 100 spectrometer, ThermoScientific, Wilmington, DE, USA) and electrophoretically (Bioanalyzer 2100; Agilent Technologies, Palo Alto, CA).

To construct Illumina-compatible libraries, we used a Kapa Hyper Prep Kit with RiboErase (Kapa Biosystems at Roche Sequencing Solutions), according to the manufacturer's instructions. In brief, total RNA was depleted of ribosomal RNA after hybridization to complementary DNA-oligonucleotides and incubation with ribonuclease H, followed by DNA digestion with DNase I. The remaining RNA was heat fragmented and hybridized with random hexamer primers for first-strand cDNA synthesis. Second-strand cDNA synthesis was performed by substituting dTTP with dUTP and adding dAMP-tails to the 3-prime ends. Different types of universal dsDNA adapters with 3-prime dTMP overhangs were ligated to the construct- allowing for multiplexing in each sequencing lane. cDNA library strand-specific amplification was performed, which excluded the dUMP-labeled strand and enabled strand-specific sequencing.

Sequencing was performed using the HiSeq 3000 platform (Illumina, San Diego, CA, USA) with 100 million paired-end reads of 150 nucleotides from each end of the RNA sequence insert, yielding double-end reads in the range of 43 to 70 million for all samples. The Bcl2fastq2 v2.17 program (Illumina) was used to demultiplex the sequencing data and convert the BCL files to FASTQ file formats. Quality control analyses of the sequencing and raw sequence data were performed using the real-time program Sequencing Analysis Viewer (Illumina) and the program FastQC (Andrews S. et al., Babraham Institute, Babraham, Camebridgeshire, UK) yielding high-quality sequencing data for a total of 21 samples constituted of 14 adnexal tumor and 7 normal samples.

All RNA sequencing data are available for download from the National Center for Biotechnology Information (NCBI) sequence reader archive (reference PRJNA492349; NCBI, National Institutes of Health, Bethesda, MD).

2.4. RNA-Seq analysis of differentially expressed genes and isoforms

The sequencing reads were first aligned to the latest UCSC transcript set (human GRCh38/hg38 at http://genome.ucsc.edu, University of California, Santa Cruz, CA, USA) using the Bowtie2 version 2.1.0 program (Ben Langmead et al., Johns Hopkins University, Baltimore, MD, USA). Quantification of gene and isoform expression was performed using the software package RSEM v1.2.15 (RNA-Seq by Expectation Maximization by Bo Li and Colin Dewey, University of Wisconsin-Madison, Madison, WI, USA).

Using the edgeR program (empirical analysis of DGE in R, by Robinson, MD et al. at https://bioconductor.org), trimmed mean of M-values (TMM) were calculated to normalize gene and transcript expression levels. The differential expression levels of uniquely aligned genes and transcripts of all 14 tumor samples versus all 7 control samples were determined (Supplemental Table 1). A statistical analysis of the 21 tissue specimens (principal component analysis and hierarchical cluster analysis) further allowed subtype analyses of the 7 control samples (N1 to N6, and N8) versus 2 subtype 1 samples of malignant adnexal tumors (T1, T7), and 12 subtype 2 samples of benign adnexal tumors (T8, T9, T11-T13, T16, and T18-T23) (Supplemental Table 2). Supplemental Tables 1 and 2 represent the human transcriptomes, with 25,343 gene transcripts and 48,009 isoform transcripts for all adnexal tumor samples, and for each of the two adnexal subtypes, including long noncoding RNA species, and excluding ribosomal, small noncoding and control RNAs. All RNA sequencing, analyses, and quality controls were performed by Technology Center for Genomics and Bioinformatics at UCLA Pathology and Laboratory Medicine, Los Angeles, CA, USA.

The whole transcriptome tables were then used to select for characteristic differentially expressed (DE) genes using the strict criteria of log2 fold change > 1, and for all adnexal tumors at false discovery rate (FDR) < 1E-8 (p-value < 5.4E-10), for subtype 1 at FDR < 2E-3 (p-values < 1.74E-4), and for subtype 2 at FDR < 1.5E-7 (p-values < 1.16E-8) (Supplemental Table 3). Gene and transcript annotations were manually updated using the NCBI Entrez Gene, ENSEMBL, and UCSC Genome Browser databases.

Next, the gene tables that were characteristic for subtype 1 (malignant adnexal tumors), and subtype 2 (benign adnexal tumors) were compared to generate 4 groups of genes and transcripts: (1) those unique to subtype 1, (2) those unique to subtype 2, (3) those common to subtypes 1 and 2 but expressed differently with ΔLog2(FC) > 0.585 (representing differences in foldchange > 1.5), and (4) those common to subtypes 1 and 2 and expressed similarly with ΔLog2(FC) < 0.585 (Supplemental Table 4).

Finally, the RNA-Seq analysis generated gene profiles characteristic for adnexal tumor subtypes 1 and 2 were compared to those for epithelial and myoepithelial ACC, which were obtained in our previously study [21]. The results are shown in Supplemental Table 5.

2.5. Cluster analysis and heatmaps

A sample similarity analysis of 14 adnexal tumor and 7 normal specimens produced a hierarchical cluster dendrogram of all detected gene and transcript expressions. Heatmaps were generated for the top 100-foldchange differentially expressed (DE) genes, including cluster analysis dendrograms from gene and sample cluster linkage similarity calculations.

2.6. Pathway analysis

Pathway core analyses and network analyses of the RNA-Seq differential expression data of the adnexal tumor subtypes were performed using the Ingenuity Pathway Analysis (IPA) program from Ingenuity Systems (Qiagen Silicon Valley, Redwood, CA, USA).

2.7. Immunohistochemical analysis

An immunohistochemical analysis (IHC) was performed on 18 samples, with antibodies against human ODAM (MyBiosource, San

Table 1
Clinico-pathological data.

	Sample	Age yrs	Sex	Location	Histological diagnosis	Tumor infiltrating lymphocytes (TILs)	Comments
1	T1	63	M	Upper back	Adnexal carcinoma	Minimal intratumoral/marked peritumoral (early tertiary lymphoid structures)	
2	T2	60	F	Scalp	Cylindroma	Minimal intratumoral	
3	T3	67	M	Scalp	Spiradenoma	Minimal intratumoral/minimal peritumoral	
4	T4	44	F	Breast	Spiradenoma	Minimal/moderate intratumoral	
5	T5	60	F	Scalp	Cylindroma	Minimal intratumoral	
6	T7	88	M	Helix	Spiradenocarcinoma	Moderate intratumoral	
7	T8	55	M	Shoulder	Spiradenoma	Moderate/marked intratumoral	
8	T9	71	F	Postauricular	Cylindroma	Minimal intratumoral/moderate peritumoral	
9	T10	76	F	Antitragus	Cylindroma	Minimal intratumoral/minimal peritumoral	
10	T11	76	F	Antitragus	Cylindroma	Minimal intratumoral/minimal peritumoral	
11	T12	40	F	Elbow	Spiradenoma	Minimal intratumoral/marked peritumoral	
12	T13	42	F	Scalp	Spiradenoma	Moderate/marked intratumoral	
13	T14	44	F	Face	Spiradenoma	Moderate/marked intratumoral	Brooke-Spiegler
14	T16	42	F	Scalp	Spiradenoma	Moderate/marked intratumoral	Brooke-Spiegler
15	T17	62	F	Pinna	Spiradenoma	Moderate intratumoral/moderate peritumoral	
16	T18	67	M	Scalp	Spiradenoma	Minimal intratumoral/moderate peritumoral	
17	T19	62	F	Arm	Spiradenoma	Moderate intratumoral/marked peritumoral (tertiary lymphoid structures)	
18	T20	66	F	Shoulder	Spiradenoma	Minimal intratumoral/moderate peritumoral	
19	T21	67	M	Scalp	Spiradenoma/cylindroma	Minimal intratumoral/minimal peritumoral	
20	T22	31	F	Scalp	Spiradenoma/cylindroma	Minimal intratumoral/minimal peritumoral	Brooke-Spiegler
21	T23	64	F	Shoulder	Spiradenoma/cylindroma	Minimal intratumoral/moderate peritumoral	Li-Fraumeni
22	T24	24	F	Scalp	Spiradenoma	Moderate intratumoral	Brooke-Spiegler

Diego, CA), HOXB13 (Antibodies-online Inc., Atlanta, GA, USA), MYB (Abcam, Cambridge, MA, USA), and SOX10 (Novus Biologicals, Littleton, CO, USA). For each protein, the results were categorized as positive (> 10% of the entire tissue specimen was positive) or negative (< 10% of the entire tissue specimen was stained), with an intensity score of 2-3+. Subcellular localization for ODAM was nuclear and cytoplasmic, while nuclear staining accounted for the other 3 biomarkers.

3. Results

3.1. Clinical and histologic data

The 22 tumors were classified as 12 spiradenomas, 5 cylindromas, 3 hybrid spiradenomas/cylindromas, 2 adnexal carcinomas. Clinical characteristics of the 22 patients are given in Table 1.

Median age at diagnosis was XX (range: 24to 88 yo). Most patients were female ($n = 16$, 73%), the more frequent primary site was in the head and neck ($n = 15$: scalp- 9, ear- 5, face- 1). The tumors' histopathological similarities and differences are illustrated in Fig. 1A and B.

The presence of lymphocytes was noted in all 22 tumors, with minimal-to-moderate intratumoral localization (Table 1).

3.2. Genome-wide RNA sequencing analysis

Differential gene expression profiles from 7 spiradenomas, 2 cylindromas, 3 hybrid spiradenomas/cylindromas, 2 adnexal carcinomas versus 7 normal adnexal skin structures were generated and compared to each other.

RNA-Seq data cluster analysis and heatmap results (Fig. 2) from all adnexal tumor samples allowed separation of two main groups, which were designated as adnexal tumor subtype 1- malignant (samples T1 and T7) subtype 2- benign (samples T8, T9, T11-T13, T16, and T18-T23) (Supplemental Table 3).

Detailed comparisons of the two tumor subtypes revealed genes and transcripts that were specific for each group and genes and transcripts that were commonly expressed in both subtypes at different or similar expression values (Supplemental Table 4).

The benign adnexal tumor samples were dominated by at least 12 development- and differentiation-related genes and transcripts. Of the top 7 highest differentially expressed (DE) signature genes, 4 (DMRTA2, HOXB13, TLX1, and SOX14) are related to development and differentiation, and 3 (ODAM, KCTD14, and CPA6) are related to signaling and protein metabolism.

In addition, we identified 8 more upregulated developmental and differentiation- related genes and transcripts that are listed in order of decreasing DE: *BARX1*, *DLX1*, *DLX2*, *HOTAIR* (HOX transcript antisense RNA), *PAX9*, *VAX2*, *ONECUT2*, and *HOXC11*. This highly varied group of development- and differentiation-related genes may correlate with a highly diverse population of adult adnexal stem cells with neoplastic features.

In contrast to this, the specific and characteristic DE genes from the malignant adnexal tumor samples had a strikingly different top 7 gene signature, represented by membrane signaling and metabolism-related proteins (*GRIA1*, *CLVS2*, *SEZ6L*, *THSD7B*, *NPTX1*, *MALRD1*), and *LHX2* as the only development and differentiation-related gene.

To identify for similarities and differences between adnexal tumors and ACC, we compared both adnexal subtypes to epithelial and myoepithelial ACC on the basis of our adnexal RNA-Seq data and data from our previous RNA-Seq study [21] (Supplemental Table 5).

The comparative analysis resulted in the highest number of specific DE genes shared between adnexal subtype 1 and epithelial ACC (36 specific genes) versus only 16 specific genes shared with myoepithelial ACC. Furthermore, the expression values of the specific genes shared between adnexal subtype 1 and epithelial ACC were all equally upregulated or downregulated, in contrast to those with myoepithelial ACC in which 2 of the 16 specific genes were oppositely regulated.

For adnexal subtype 2, the highest number of shared specific DE genes was observed for myoepithelial ACC (27 specific genes), which was only slightly higher than that for epithelial ACC with (21 shared specific genes). In adnexal tumor subtype 2, several of the shared specific genes are oppositely regulated, with 10 of 27 (37%) oppositely expressed in myoepithelial ACC, and 6 of the 21 (29%) specific genes oppositely expressed in epithelial ACC.

These comparisons indicate a strong similarity between adnexal subtype 1 (malignant) and epithelial ACC and a weak similarity between adnexal subtype 2 (benign) and myoepithelial ACC rather than with epithelial ACC.

3.3. Biomarker analysis

To validate the gene expression patterns of the adnexal tumor types detected by RNA-Seq analysis, we characterized the protein expression levels of 4 selected genes by immunohistochemistry (IHC). The 4 antibodies were selected on the basis of the specificity and upregulation of

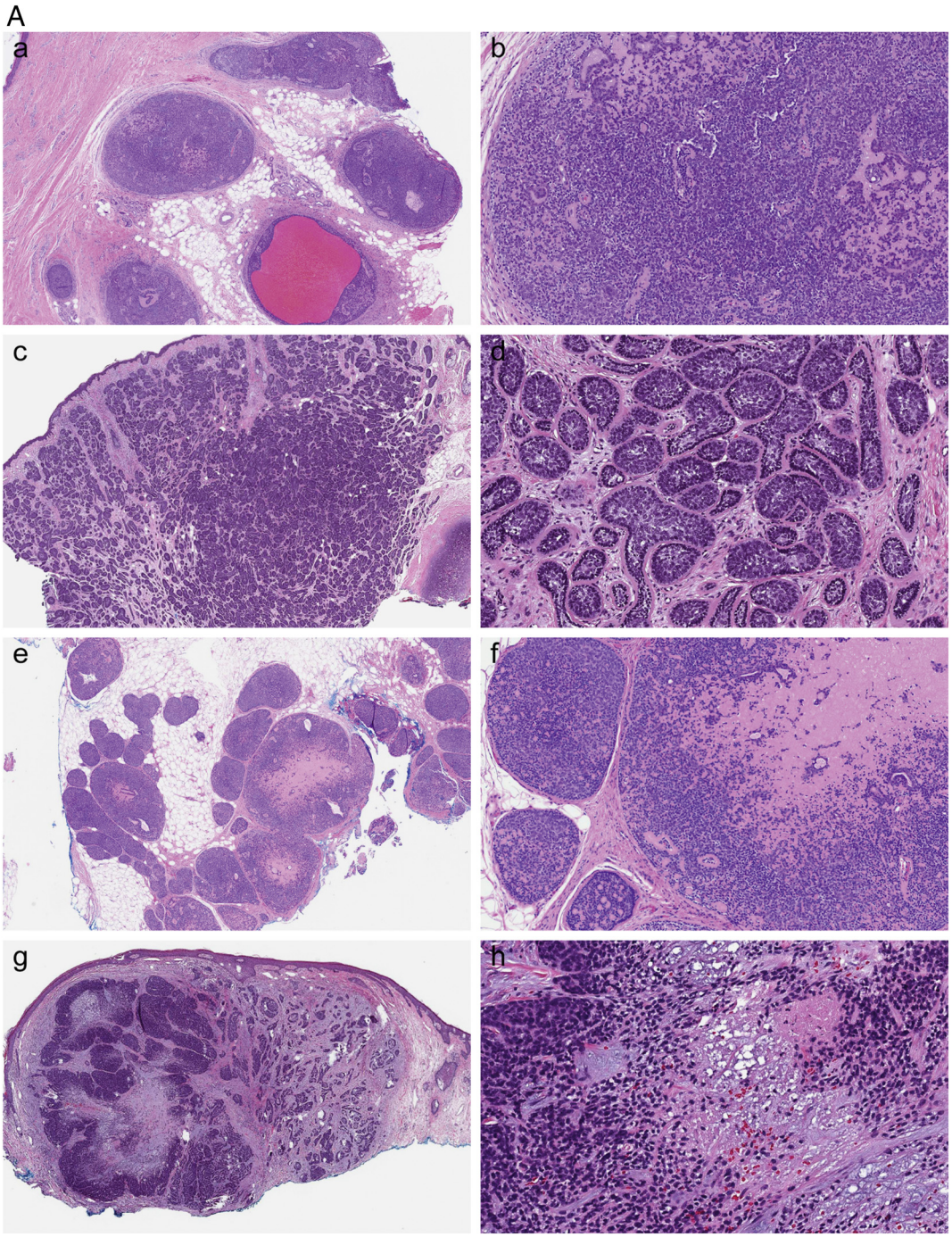

Fig. 1. A. Histopathological similarities and differences. **Spiradenoma** (**a**, **b**). At scanning power, the silhouette of spiradenoma is distinctive, with typically relatively few large, round, smooth-bordered aggregations of epithelial cells. **Cylindroma** (**c**, **d**). The histopathologic features of cylindroma are very much like those of spiradenoma but differ in silhouette at scanning power. The aggregations were more numerous and smaller, packed together in a "jigsaw puzzle" pattern. **Spiradenocylindroma** (**e**, **f**). Collision between spiradenoma and cylindroma. **Eccrine spiradenocarcinoma** (**g**, **h**). Presence of focal necrosis, increased mitotic activity and stromal reaction associated with infiltrative growth (T7). Panel **B**. The other adnexal carcinomas (T1) displayed features of eccrine spiradenoma (b, e), basal cell carcinoma (a, f), trichoblastoma (c, d) and focal sebaceous differentiation. This sample segregated at the gene expression level, as noted from the heat maps and cluster analysis.

their genes for the adnexal tumor types and the availability of high-quality antibodies. This resulted in the selection of genes that were specific for adnexal subtype 2: ODAM, HOXB13 with Log2 fold changes (Log2(FC)) of 10.02 and 8.65, respectively; and, SOX10 with Log2(FC) for adnexal tumor type 1 = 2.82 and for type 2 = 4.06, and MYB with Log2(FC) for adnexal tumor type 1 = 2.57 and for type 2 = 3.24, which were commonly expressed in all adnexal tumors (Supplemental Table 4).

The IHC analysis of the expressed proteins revealed that *ODAM* was positive in 83%, *SOX10* in 89%, and *HOXB13* and *MYB* each 67%, of tested tumors. The expression of these biomarkers was absent or occasionally present in eccrine glands from normal skin though *ODAM* expression was noted in basal cells and dermal trichilemmal cells from normal skin. A representative illustration of the selected biomarkers is shown in Fig. 3 and detailed IHC analysis results are given in Table 2.

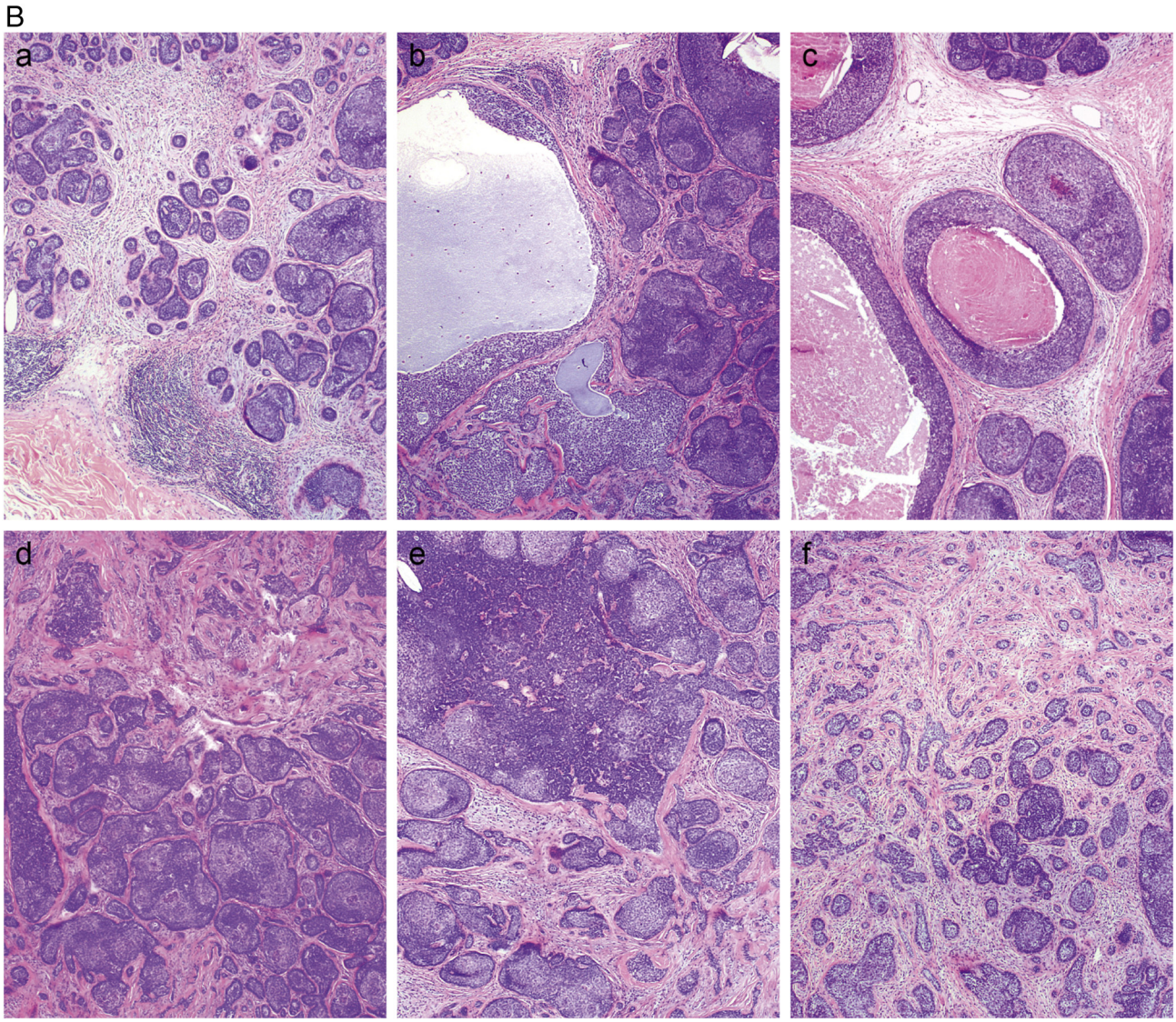

Fig. 1. (*continued*)

3.4. Pathway analysis

IPA pathway core analysis of adnexal tumor subtype 1 as well as for subtype 2 revealed the highest score for cancer as result of the top diseases and top biological functions.

For adnexal tumor subtype 1, IPA determined the top network associated with embryonic development, endocrine system development and function, and organ development; the network pathway included associations between upregulated LHX2 and WNT signaling (Fig. 4A). For adnexal tumor subtype 2, IPA determined the top network associated with embryonic development, organismal development, and tissue development; the network pathway included associations between the overexpressed developmental and the differentiation-related transcription factors SOX4, SOX10, SOX11 and DLX2 (Fig. 4B).

4. Discussions

In this study, we performed an RNA-Seq analysis of FFPE skin adnexal neoplasms and identified the genes and transcripts that define these neoplastic tissues with insights into their histogenesis.

The synchronous occurrence of follicular, sebaceous, or apocrine differentiation in cutaneous adnexal neoplasms is a known event, more often encountered in benign neoplasms. There have been only anecdotal reports of cutaneous malignant adnexal tumors with multilineage differentiation [22]. These cases illustrate the spectrum of diversity encountered in malignant proliferations, with differentiation toward the folliculosebaceous-apocrine unit [22]. One of the adnexal carcinomas (T1) in our study displayed features of eccrine spiradenoma, basal cell carcinoma, trichoblastoma, and focal sebaceous differentiation. This sample obviously segregated at the gene expression level, as noted from the heatmaps and cluster analysis. The other adnexal carcinoma (T7) had eccrine spiradenocarcinoma morphologic features, and although the heatmap highlighted gene expression differences, this tumor clustered together with T23 (hybrid spiradenoma/cylindroma) and T18 (spiradenoma) and thus had an eccrine progenitor. The next cluster included T19 (spiradenoma), T8 (spiradenoma), and T22 (hybrid spiradenoma/cylindroma). The dominant group of 7 tumors included 3 spiradenomas (T20, T16, and T13), 3 cylindromas (T9, T12, and T11) and 1 hybrid spiradenoma/cylindroma (T21).

Historically, spiradenoma has been described as eccrine in origin, dating back to the largest case series published (134 cases in 1956) from The Armed Forces Institute of Pathology (AFIP) [2]. The histogenesis of cylindroma was also promoted as eccrine by AFIP [1,3,23] and is equally controversial. Several studies have supported a folliculosebaceous lineage, on the basis of the results of immunohistochemical studies

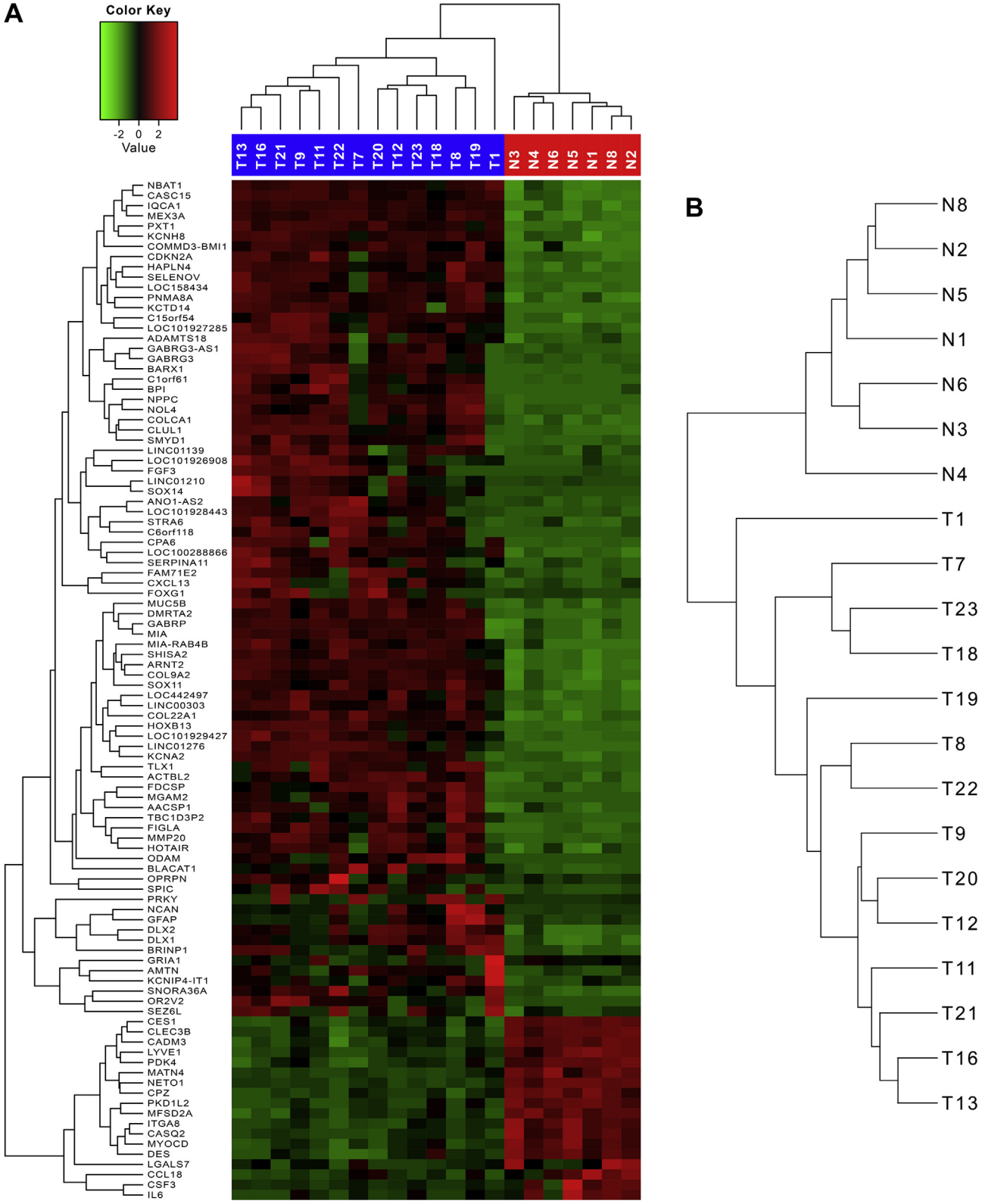

Fig. 2. A. Heatmap of the top 100 highest differentially expressed genes and transcripts with dendrograms for the samples and genes.
B. The cluster dendrogram shows similarities between the neoplastic adnexal samples and normal samples.

[24,25]. Arguments in support of folliculosebaceous-apocrine unit derivation include the frequent co-localization of spiradenoma and cylindroma with trichoepithelioma in patients with Brooke-Spiegler syndrome, the association of cylindromas with trichoepitheliomas and milia in patients with Rasmussen syndrome, and the anatomical location of spiradenomas and cylindromas, in contrast to poromas, which do not occur in areas rich in eccrine glands, such as the palms and soles, but instead favor locations rich in hair follicles, such as the face and scalp (reviewed in Sellheyer [24]).

Sellheyer focused the analysis on CD200 and the presence of local

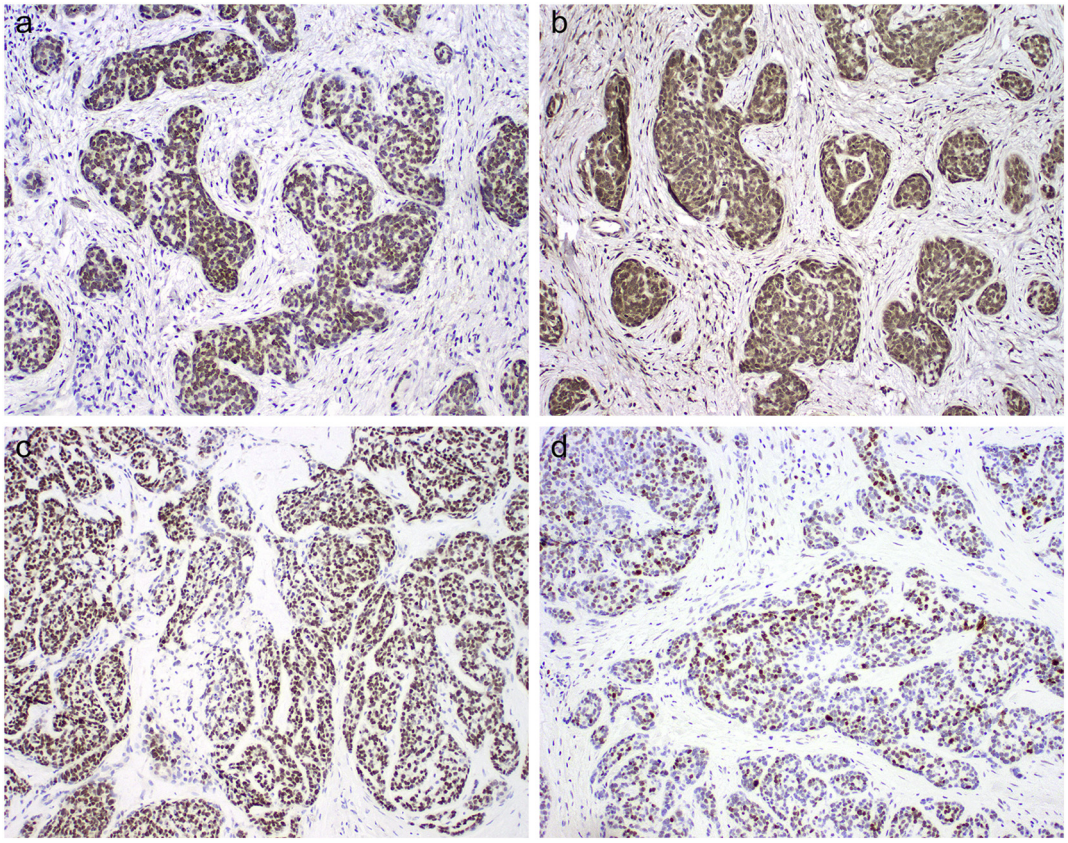

Fig. 3. The gene expression patterns detected by RNA sequencing analysis were validated using IHC analysis and the protein expression levels of 4 selected genes. Immunoperoxidase studies were conducted using antibodies against homeobox protein Hox-B13 (a), odontogenic ameloblast-associated protein Odam (b), SRY-related HMG-box Sox10 (c), and myeloblastosis transcription factor Myb (d).

immune response [24]. The stem cell marker transmembrane glycoprotein CD200 represents an immunoprotective membranous molecule that is highly specific for the hair follicle bulge. The author reported the presence of numerous lymphocytes within the epithelial component of both spiradenomas and cylindromas, as well as the absence or rare presence of lymphocytes that were confined to stroma in hidradenoma, poroma, dermal duct tumor, and hidroacanthoma simplex. CD200 and the lymphocytes that represent the immunoregulatory cells found in spiradenomas and cylindromas may be somehow associated with the histogenesis or immunosurveillance of these adnexal neoplasms [24]. The hair follicle bulge represents a site of relative immune privilege; when the immunoprotection of the bulge area gets out of control, a cutaneous malignancy or an adnexal tumor may develop (reviewed in Sellheyer [24]). On the basis of the expression of stem cell markers in the tumors examined in Sellheyer's study (mainly CD200), it was concluded that both spiradenoma and cylindroma are not eccrine but follicular tumors [24].

Our RNA-Seq analysis of adnexal tumors reveals the highest

Table 2
Biomarker validation and detailed immunohistochemistry analysis.

Sample ID	HOX B13 67%	ODAM 83%	SOX10 89%	MYB 67%
T1	Negative	Positive	Negative	Negative (< 5%)
T5	Positive (30%)	Negative	Negative	Positive (30%)
T7	Negative	Positive	Positive (> 80%)- basal	Negative (< 5%)
T8	Negative	Positive	Positive (> 80%)- basal	Negative
T9	Positive (80%)	Positive	Positive (> 80%)- basal	Positive (30%)
T10	Negative (< 5%)	Positive	Positive (> 80%)	Positive (50%)
T11	Positive (30%)	Positive	Positive (> 80%)	Positive (50%)
T12	Negative	Positive	Positive (> 80%)- basal	Positive (20%)
T13	Positive (30%)	Positive	Positive (> 80%)- basal	Positive (80%)
T14	Positive (30%)	Negative	Positive (> 80%)- basal	Positive (30%)
T16	Positive (30%)	Positive	Positive (> 80%)- basal	Positive (30%)
T17	Positive (50%)	Positive	Positive (> 80%)- basal	Positive (50%)
T18	Positive (30%)	Positive	Positive (> 80%)- basal	Negative
T19	Positive (80%)	Positive	Positive (> 80%)- basal	Negative
T20	Positive (30%)	Positive	Positive (> 80%)- basal	Positive (20%)
T21	Positive (30%)	Positive	Positive (> 80%)- basal	Positive (30%)
T22	Negative (< 5%)	Positive	Positive (> 80%)- basal	Positive (50%)
T23	Positive (30%)	Negative	Positive (> 80%)- basal	Negative (< 5%)

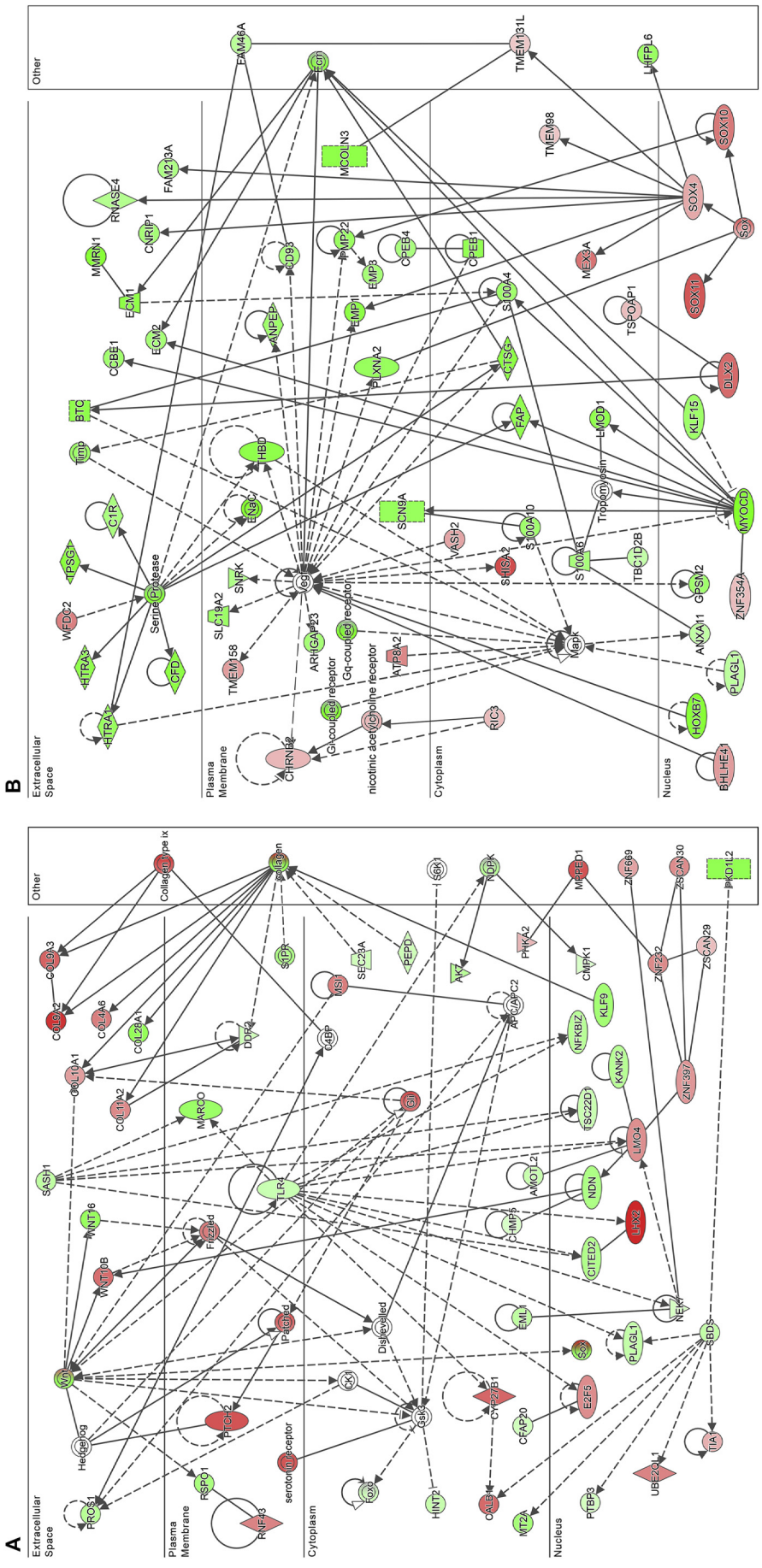

Fig. 4. A. The highest scoring IPA pathway network for adnexal tumor type 1, including LHX2-regulated WNT signaling. **B.** The highest scoring IPA pathway network for adnexal tumor type 2, including the development- and differentiation-related transcription factors SOX4, SOX10, SOX11 and DLX2.

expressed genes and transcripts were predominantly development- and differentiation-related genes and transcripts with ODAM, KCTD14, DMRTA2, HOXB13, TLX1, SOX14, and HOTAIR specific for subtype 2; LHX2 specific for subtype 1, and SOX11, SOX10, SOX8, IRX4, LEF1 (lymphoid enhancer-binding factor 1) and MYB common in all adnexal tumors (Supplementary Table 4).

The biological functions of some of these genes are described here to categorize them as biomarkers for these adnexal tumors.

ODAM, odontogenic ameloblast associated, (Log2(FC) 10.02) is involved in odontogenesis of dentin-containing tooth, the regulation of actin cytoskeleton organization, and the positive regulation of GTPase activity, as well as in inflammatory response and gene expression. The ODAM protein inhibits the growth and migration of human melanoma cells and elicits *PTEN* elevation and inactivation of *PI3K/AKT* signaling [26]. ODAM has been proposed to have diverse functions that vary with protein location in various cell lines. Nuclear *ODAM* appears to be associated with *MMP-20* regulation and tumorigenesis [27], whereas other functions may take place in the cytoplasm and extracellular matrix [27]. Ectopic *ODAM* expression in melanoma cell lines suppresses growth and migratory activity in these cells while initiating elevated *PTEN* expression and *AKT* activity suppression [26]. *ODAM* expression maintains cancer cell adhesion, resulting in the prevention of metastasis via the regulation of *RhoA* signaling in breast cancer cells [28] and inhibition of breast cancer tumorigenesis [29].

LHX2 may be involved in the overexpression of WNT10B to activate WNT signaling [30], and this probably contributes to the cancer stem cell features and the malignancy of this adnexal tumor type. This might be corroborated by the discovery of the LHX2 - WNT10B pathway in stem cells from epithelial keratinocytes that reside in the outermost bulge layer of hair follicles [31], thus indicating that a similarity exists between the adnexal tumor subgroup 1 and epithelial hair follicle stem cells.

The intronless gene SOX11, SRY (sex determining region Y)-box 11, (Log2(FC) 5.54) encodes a member of the SOX (SRY-related HMG (High Mobility Group)-box) family of transcription factors that are involved in the regulation of embryonic development and the determination of cell fate. The encoded protein may act as a transcriptional regulator after forming a protein complex with other proteins and may function in the developing nervous system and play a role in tumorigenesis [32-34].

LEF1, (Log2(FC) 3.5) belongs to a family of proteins that share homology with the high mobility group protein-1 (HMGB1) and can bind to a functionally important site in the T-cell receptor-alpha enhancer, conferring maximal enhancer activity. The LEF1 transcription factor is involved in the WNT signaling pathway and may function in hair cell differentiation and follicle morphogenesis [35-37]. Mutations in the LEF1 gene have been found in somatic sebaceous tumors [38,39] and basal cell carcinoma [40]. The LEF1 gene has also been linked to other cancers, including androgen-independent prostate cancer [41]. Alternative splicing results in multiple transcript variants.

HOTAIR, (Log2(FC) 4.43) is located within the homeobox C (HOXC) gene cluster on chromosome 12 and is co-expressed with HOXC genes. HOTAIR functions as a noncoding RNA transcript, and is the first lncRNA that has been identified to regulate genes from a far distance in its subcellular localization within the nucleus and cytoplasm. The HOTAIR transcript binds lysine-specific demethylase 1 (LSD1) and polycomb repressive complex 2 (PRC2) and serves as a scaffold to assemble these regulators at the HOXD gene cluster, thereby promoting epigenetic repression of HOXD. The HOTAIR lncRNA is highly expressed in multiple tumors [42,43], including breast cancer, gastric cancer, liver cancer, sarcoma and nasopharyngeal cancer, where it promotes cancer cell proliferation, invasion and metastasis, while inhibiting apoptosis. HOTAIR-knockout can reduce tumor growth. As a result, HOTAIR has been suggested to be an oncogene. HOTAIR is known to modulate the cancer epigenome and reprogram the chromatin state. Specifically, HOTAIR binds PRC2 and lysine-specific demethylase 1 (LSD1) forming a HOTAIR-PRC2-LSD1 complex that targets and silences genes of the HOXD locus on chromosome 2, including genes that are involved in the suppression of metastasis by silencing the genes HOXD10, MMP1/3, PTEN, SNAI1/2 (snail1/2), and WIF-1. Conversely, depletion of HOTAIR ncRNA by RNA interference in primary human fibroblasts leads to dramatic transcriptional activation across 40 kb of the HOXD locus on chromosome 2, including HOXD8, HOXD9, HOXD10, HOXD11, and multiple ncRNAs.

Similar to ACC of the salivary gland, the *MYB-NFIB* gene fusion product, as a result of t(6;9)(q22-23;p23-24) translocation, has been shown in a subset of dermal cylindromas with overexpression of MYB protein [16,44,45]. In this study, the MYB RNA transcript was expressed at a higher level in the benign adnexal tumor type 2 at higher DE values (Log2(FC) 3.24) than in the malignant adnexal tumor subtype 1 (Log2(FC) 2.57). The *MYB* protein was expressed in 67% of tumors (positive in all tested cylindromas and hybrids, and positive in 5 of 8 tested spiradenomas), with very focal MYB expression of < 5% (scored as negative) in both adnexal carcinomas.

Loss of MYB expression in the malignant components of spiradenomas was reported by van der Horst and collaborators [16]. In our unpublished experience, MYB is not an entirely specific biomarker for ACC and adnexal tumors (mainly cylindromas), with immunoreactivity occasionally seen in basal cell carcinoma and other basaloid neoplasms.

Similarly, SOX10 expression, which is mainly confined to myoepithelial cells and basal cells in various biphasic salivary and adnexal tumors, is known and accounts for less specificity as a biomarker. Of the 18 cases in our IHC analysis, 89% had SOX10 immunoreactivity, which was mainly confined to basal cells.

Although engrailed homeobox 1 (EN1) was not detected in the top 100 strongly differentially expressed genes, given the morphological overlap between eccrine adnexal tumors and ACC, we tested the immunoreactivity between these tumors and anti-EN1. Two spiradenomas (T14 and T17) showed EN1 expression, while the other samples were negative or had weak expression. Our previous experience with high expression of EN1 in ACC shows a reliable correlation between transcriptome, methylation, and protein expression [21,46,47]. Miura et al. [48] recently reported on the EN1 protein expression in most of the tumor cells of sweat gland neoplasms with eccrine gland differentiation, while negative in sebaceous and hair follicle neoplasms.

We further compared the transcriptome of eccrine adnexal tumors with the transcriptome of ACCs reported in our previous study [21], to identify the overlapping genes that may indicate histogenesis. There were 36 specific genes overlapping between adnexal tumor type 1 and the epithelial-dominant subtype of ACC, including TBX1, CBX8, FOXM1, and FOXO3, and 27 specific genes overlapping adnexal tumor type 2 with the myoepithelial-dominant subtype of ACC, including ODAM, DPP4 (T cell activation antigen CD26), and TP53 (Supplemental Table 5). At this point there is no known specific biomarker to aid in the diagnosis of eccrine spiradenoma and cylindroma in small samples or biopsies within the context of morphological overlap with ACC.

In conclusion, spiradenomas and cylindromas seem to be mainly defined by the high number of overexpressed developmental genes, mostly homeobox genes, which provide the potential for transformation and plasticity, though these tumors are also defined by the differentiation and proliferation behavior of their neoplastic cells. These data may help us understand the contribution of different adnexal epithelial cell types to the etiology and molecular pathology of dermal adnexal disease.

Supplementary data to this article can be found online at https://doi.org/10.1016/j.anndiagpath.2019.04.015.

Acknowledgements

This study was supported by MD Anderson Cancer Center start-up funds (DB). The authors declare no conflict of interest.

References

[1] Crain RC, Helwig EB. Dermal cylindroma (dermal eccrine cylindroma). Am J Clin Pathol 1961;35:504–15. Jun.
[2] Kersting DW, Helwig EB. Eccrine spiradenoma. AMA Arch Derm Mar 1956;73(3):199–227.
[3] Urbach F, Graham JH, Goldstein J, Munger BL. Dermal eccrine cylindroma: a histochemical, electron microscopic, and therapeutic (X-ray) study. Arch Dermatol 1963;88:880–94. Dec.
[4] Alsaad KO, Obaidat NA, Ghazarian D. Skin adnexal neoplasms–part 1: an approach to tumours of the pilosebaceous unit. J Clin Pathol 2007;60(2):129–44. Feb.
[5] Brenn T. Diagnostic challenges in dermatopathology. Surg Pathol Clin 2017;10(2):xi–. Jun.
[6] Mambo NC. Eccrine spiradenoma: clinical and pathologic study of 49 tumors. J Cutan Pathol 1983;10(5):312–20. Oct.
[7] Obaidat NA, Alsaad KO, Ghazarian D. Skin adnexal neoplasms–part 2: an approach to tumours of cutaneous sweat glands. J Clin Pathol 2007;60(2):145–59. Feb.
[8] Kazakov DV. Brooke-Spiegler syndrome and phenotypic variants: an update. Head Neck Pathol Jun 2016;10(2):125–30.
[9] Kazakov DV, Zelger B, Rutten A, et al. Morphologic diversity of malignant neoplasms arising in preexisting spiradenoma, cylindroma, and spiradenocylindroma based on the study of 24 cases, sporadic or occurring in the setting of Brooke-Spiegler syndrome. Am J Surg Pathol 2009;33(5):705–19. May.
[10] van der Horst MPJ, Brenn T. Update on malignant sweat gland tumors. Surg Pathol Clin Jun 2017;10(2):383–97.
[11] Sima R, Vanecek T, Kacerovska D, et al. Brooke-Spiegler syndrome: report of 10 patients from 8 families with novel germline mutations: evidence of diverse somatic mutations in the same patient regardless of tumor type. Diagn Mol Pathol Jun 2010;19(2):83–91.
[12] Andreoli MT, Itani KM. Malignant eccrine spiradenoma: a meta-analysis of reported cases. Am J Surg 2011;201(5):695–9. May.
[13] Jacquemus J, Dalle S, Faure M, Chouvet B, Beatrix O, Balme B. Malignant transformation of an eccrine spiradenoma. Ann Dermatol Venereol 2017;144(3):203–7. Mar.
[14] McCluggage WG, Fon LJ, O'Rourke D, et al. Malignant eccrine spiradenoma with carcinomatous and sarcomatous elements. J Clin Pathol 1997;50(10):871–3. Oct.
[15] Mirza I, Kloss R, Sieber SC. Malignant eccrine spiradenoma. Arch Pathol Lab Med 2002;126(5):591–4. May.
[16] van der Horst MP, Marusic Z, Hornick JL, Luzar B, Brenn T. Morphologically low-grade spiradenocarcinoma: a clinicopathologic study of 19 cases with emphasis on outcome and MYB expression. Mod Pathol 2015;28(7):944–53. Jul.
[17] Crowson AN, Magro CM, Mihm MC. Malignant adnexal neoplasms. Mod Pathol 2006;19(Suppl. 2):S93–126. Feb.
[18] Dabska M. On malignant transformation of eccrine spiradenoma. Nowotwory 1971;21(1):37–45. Jan-Mar.
[19] Dabska M. Malignant transformation of eccrine spiradenoma. Pol Med J 1972;11(2):388–96.
[20] Petersson F, Kutzner H, Spagnolo DV, et al. Adenoid cystic carcinoma-like pattern in spiradenoma and spiradenocylindroma: a rare feature in sporadic neoplasms and those associated with Brooke-Spiegler syndrome. Am J Dermatopathol 2009;31(7):642–8. Oct.
[21] Bell D, Bell AH, Bondaruk J, Hanna EY, Weber RS. In-depth characterization of the salivary adenoid cystic carcinoma transcriptome with emphasis on dominant cell type. Cancer May 15 2016;122(10):1513–22.
[22] Kazakov DV, Kutzner H, Mukensnabl P, Michal M. Low-grade adnexal carcinoma of the skin with multidirectional (glandular, trichoblastomatous, spiradenocylindromatous) differentiation. Am J Dermatopathol 2006;28(4):341–5. Aug.
[23] Munger BL, Graham JH, Helwig EB. Ultrastructure and histochemical characteristics of dermal eccrine cylindroma (turban tumor). J Invest Dermatol 1962;39:577–95. Dec.
[24] Sellheyer K. Spiradenoma and cylindroma originate from the hair follicle bulge and not from the eccrine sweat gland: an immunohistochemical study with CD200 and other stem cell markers. J Cutan Pathol 2015;42(2):90–101. Feb.
[25] Winkelmann RK, Wolff K. Histochemistry of hidradenoma and eccrine spiradenoma. J Invest Dermatol 1967;49(2):173–80. Aug.
[26] Foster JS, Fish LM, Phipps JE, et al. Odontogenic ameloblast-associated protein (ODAM) inhibits growth and migration of human melanoma cells and elicits PTEN elevation and inactivation of PI3K/AKT signaling. BMC Cancer May 7 2013;13:227.
[27] Lee HK, Park SJ, Oh HJ, Kim JW, Bae HS, Park JC. Expression pattern, subcellular localization, and functional implications of ODAM in ameloblasts, odontoblasts, osteoblasts, and various cancer cells. Gene Expr Patterns 2012;12(3–4):102–8. Mar-Apr.
[28] Lee HK, Choung HW, Yang YI, Yoon HJ, Park IA, Park JC. ODAM inhibits RhoA-dependent invasion in breast cancer. Cell Biochem Funct 2015;33(7):451–61. Oct.
[29] Kestler DP, Foster JS, Bruker CT, et al. ODAM expression inhibits human breast cancer tumorigenesis. Breast Cancer (Auckl) 2011;5:73–85.
[30] Bohr S, Patel SJ, Vasko R, et al. Highly upregulated Lhx2 in the Foxn1 −/− nude mouse phenotype reflects a dysregulated and expanded epidermal stem cell niche. PLoS One 2013;8(5):e64223.
[31] Lim X, Nusse R. Wnt signaling in skin development, homeostasis, and disease. Cold Spring Harb Perspect Biol Feb 1 2013;5(2).
[32] Bhattaram P, Kato K, Lefebvre V. Progenitor cell fate, SOXC and WNT. Oncotarget Sep 22 2015;6(28):24596–7.
[33] Kuo PY, Leshchenko VV, Fazzari MJ, et al. High-resolution chromatin immunoprecipitation (ChIP) sequencing reveals novel binding targets and prognostic role for SOX11 in mantle cell lymphoma. Oncogene Mar 5 2015;34(10):1231–40.
[34] Zhang YH, Liu J, Dawlett M, Guo M, Sun X, Gong Y. The role of SOX11 immunostaining in confirming the diagnosis of mantle cell lymphoma on fine-needle aspiration samples. Cancer Cytopathol 2014;122(12):892–7. Dec.
[35] Giles RH, van Es JH, Clevers H. Caught up in a Wnt storm: Wnt signaling in cancer. Biochim Biophys Acta Jun 5 2003;1653(1):1–24.
[36] Hoppler S, Kavanagh CL. Wnt signalling: variety at the core. J Cell Sci Feb 1 2007;120(Pt 3):385–93.
[37] Widelitz RB. Regulating the regulators: routing the Wnt-beta-catenin–Lef signals. J Invest Dermatol Aug 2004;123(2):VIII–.
[38] Merrill BJ, Gat U, DasGupta R, Fuchs E. Tcf3 and Lef1 regulate lineage differentiation of multipotent stem cells in skin. Genes Dev Jul 1 2001;15(13):1688–705.
[39] Niemann C, Owens DM, Schettina P, Watt FM. Dual role of inactivating Lef1 mutations in epidermis: tumor promotion and specification of tumor type. Cancer Res Apr 1 2007;67(7):2916–21.
[40] Kriegl L, Horst D, Kirchner T, Jung A. LEF-1 expression in basal cell carcinomas. Br J Dermatol 2009;160(6):1353–6. Jun.
[41] Wu X, Daniels G, Shapiro E, et al. LEF1 identifies androgen-independent epithelium in the developing prostate. Mol Endocrinol 2011;25(6):1018–26. Jun.
[42] Wang Y, Dang Y, Liu J, Ouyang X. The function of homeobox genes and lncRNAs in cancer. Oncol Lett 2016;12(3):1635–41. Sep.
[43] Yu X, Li Z. Long non-coding RNA HOTAIR: a novel oncogene (review). Mol Med Rep 2015;12(4):5611–8. Oct.
[44] Evangelista MT, North JP. MYB, CD117 and SOX-10 expression in cutaneous adnexal tumors. J Cutan Pathol 2017;44(5):444–50. May.
[45] Rajan N, Andersson MK, Sinclair N, et al. Overexpression of MYB drives proliferation of CYLD-defective cylindroma cells. J Pathol Jun 2016;239(2):197–205.
[46] Bell A, Bell D, Weber RS, El-Naggar AK. CpG island methylation profiling in human salivary gland adenoid cystic carcinoma. Cancer Jul 1 2011;117(13):2898–909.
[47] Bell D, Bell A, Roberts D, Weber RS, El-Naggar AK. Developmental transcription factor EN1–a novel biomarker in human salivary gland adenoid cystic carcinoma. Cancer Mar 1 2012;118(5):1288–92.
[48] Miura K, Akashi T, Ando N, et al. Homeobox transcriptional factor engrailed homeobox 1 is expressed specifically in normal and neoplastic sweat gland cells. Histopathology 2018;72(7):1199–208. Jun.